PLANAR INDUCTOR DESIGN FOR HIGH POWER APPLICATIONS

A. Eroglu[*]

Department of Engineering, IPFW, 2101 E. Coliseum Blvd., Fort Wayne, IN 46805, USA

Abstract—Design, simulation, and implementation of low profile microstrip spiral inductors for high power Industrial, Scientific and Medical (ISM) applications at the high frequency (HF-3–30 MHz) range are given for the first time. An accurate analytical model and algorithm have been developed to determine the simplified lumped element equivalent model parameters for spiral inductor and its physical dimensions. Five different spiral inductors are then simulated with a planar electromagnetic simulator using the physical dimensions obtained for the desired inductance values with the analytical method. The implementation method and substrate selection for spiral inductors at the HF range are given in detail for high power applications. The spiral inductors are then constructed on 100 mil Alumina substrate and measured with network analyzer. It is found that analytical, simulation and measurement results are in close agreement and the analytical method and algorithm that have been developed can be used to accurately determine the physical dimensions, and the resonant frequency of the spiral inductor for the desired inductance value.

1. INTRODUCTION

There is an increasing demand in the area of radio frequency applications to use cost effective planar inductors. Spiral type planar inductors are widely used in the design of power amplifiers, oscillators, microwave switches, combiners, and splitters, etc. for ISM applications at the HF (high frequency) range. There have been numerous publications on spiral inductor design at microwave frequencies. Significant portion of the related work on spiral inductors is dedicated

* Corresponding author: Abdullah Eroglu (eroglua@ipfw.edu).

to design spiral inductors at microwave frequencies using substrates such as Silicon (Si) [1–5] or gallium-arsenide (GaAs) [6–8]. A modeling technique using time domain (TD) impulse to characterize microwave spiral inductors is proposed in [9]. LTCC spiral inductor design using the synthesis method is outlined in [10]. Chip spiral inductor design which is mostly valid for CMOS processes is given in [11]. In [12], design of the spiral inductors using layout synthesis and optimization technique on a crystalline polymer substrate is discussed. Nano-spiral inductor design for low power digital spintronic circuits is presented in [13]. The inductance of the spiral inductor is calculated using Greenhouse-based formulation is given in [14–16]. Other methods such as empirical formulation in calculation of the inductance of the spirals are outlined in [17]. The inductance of the spiral using a mathematical model with Kramers–Kronig relations are proposed in [18]. There have been also reports for calculating the spiral inductor parameters based on the measured S-parameters [19, 20]. Numerical methods such as finite difference time domain method (FDTD) and multi resolution time domain method (MRTD) [21, 22] have been also applied for characterization of the spiral inductors. However, none of the publications reported presents an analytical model for the design of spiral inductors at HF (3 MHz–30 MHz) range for high power ISM applications. HF range is a common frequency range that is used for ISM (Industrial, scientific, and medical) applications. Spiral inductors, when used in ISM applications, must be designed to handle power in the range of several kilowatts. They should demonstrate good thermal characteristics, sustained inductance value and low loss under such high power because any change in the component values in RF system affects the performance and can cause catastrophic failures. This can be prevented by application of an accurate design method for the material that is used as a substrate.

In this paper, practical and accurate analytical design method and algorithm for low profile microstrip spiral inductors are proposed using the simplified lumped element equivalent model. The method and algorithm are used to obtain the physical dimensions and resonant frequency of the spiral inductors for the desired inductance values. The physical dimensions are then used to simulate the spiral inductors by planar electromagnetic simulator, Sonnet, to validate the design parameters. Spiral inductors are then implemented on 100 mil thick Alumina (Al_2O_3) substrate using the implementation method proposed for the required level of power dissipation. Network analyzer, HP8753ES, is used to measure the inductance values and resonant frequencies of the spiral inductors. It has been seen that the results obtained by the developed analytical method and algorithm are in

agreement with simulation and experimental results.

2. ANALYTICAL DESIGN METHOD FOR SPIRAL INDUCTOR AT HF RANGE

2.1. Design Equations

The inductance value of the spiral inductors at the HF range can be determined using the quasi-static method proposed by Greenhouse [14] with a good level of accuracy.

The method in [14] takes into account of self coupling, and mutual coupling between each trace. The layout of the two conductors that is used in the inductance calculation is illustrated in Fig. 1(a). *GMD* is the geometric mean distance between two conductors and *GMD* represents the arithmetic mean distance between two conductors. The total inductance of the configuration of the spiral inductor is

$$L_T = L_0 + \Sigma M \tag{1a}$$

where L_T is the total inductance, L_0 is the sum of the self inductances, and ΣM is the sum of the total mutual inductances. The application of the formulation given by (1) can be demonstrated for the spiral inductor illustrated in Figs. 1(b) and 1(c) as

$$L_T = L_1 + L_2 + L_3 + L_4 + L_5 - 2\left(M_{13} + M_{24} + M_{35}\right) + 2M_{15} \tag{1b}$$

The general relations that can be used in the algorithm for the spiral inductance calculation then become

$$L_i = 0.0002 l_i \left[\ln\left(2\frac{l_i}{GMD}\right) - 1.25 + \frac{AMD}{l_i} + \frac{\mu}{4}T \right] \tag{2}$$

$$M_{ij} = 0.0002 l_i Q_i \tag{3}$$

$$\ln(GMD_i) = \ln(d) - \frac{1}{12\left(\frac{d}{w}\right)^2} - \frac{1}{60\left(\frac{d}{w}\right)^4} - \frac{1}{168\left(\frac{d}{w}\right)^6} - \frac{1}{360\left(\frac{d}{w}\right)^8} - \dots \tag{4}$$

$$Q_i = \ln\left[\frac{l_i}{GMD_i} + \left(1 + \left(\frac{l_i}{GMD_i}\right)^2\right)^{0.5} \right] - \left(1 + \left(\frac{GMD_i}{l_i}\right)^2\right)^{0.5} + \frac{GMD_i}{l_i} \tag{5}$$

$$AMD = w + t \tag{6}$$

where L_i is the self inductance of the segment i, M_{ij} is the mutual inductance between segments i and j, l_i is the length of segment l_i, μ is the permeability of the conductor, T is the frequency correction factor, d is the distance between conductor filaments, w is the width of the conductor, t is the thickness of the conductor, Q_i is the mutual
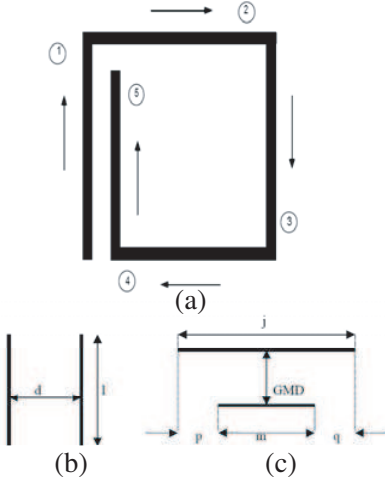
(a)

(b)   (c)

Figure 1. (a) Rectangular spiral inductor. (b) Layout of current filaments. (c) Two-parallel filament geometry.
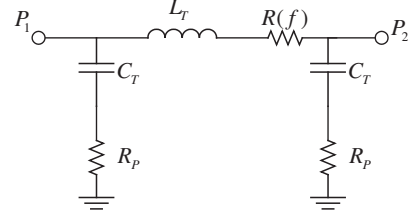

Figure 2. Two-port lumped-element equivalent circuit for spiral inductor.

inductance parameter of segment i, GMD_i is the geometric distance of segment i, and GMD is the arithmetic mean distance.

The two port lumped element equivalent circuit for a spiral inductor at the HF range is represented by a π network shown in Fig. 2.

C_T is the lumped element equivalent circuit capacitance that has the effect of odd mode, even mode and interline coupling capacitances between coupled lines of the spiral inductor. The spiral inductor is separated into segments for overall capacitance calculation. The lines that are coupled and used for odd mode, even mode and interline coupling capacitances calculation are circled in Fig. 3. One half of the spiral inductor is used for the calculation of C_T due to symmetry.

The capacitance calculation for additional segments that are out of symmetric structure of the spiral inductor has to be performed and added to overall capacitance. The capacitance between spiral segments is found from the equivalent circuit shown in Fig. 4.

C_e is the even mode capacitance, C_o is the odd mode capacitance and C_c is the interline coupling capacitance in Fig. 4. The calculation of the even and mode capacitances are given in detail in [23, 24]. The interline coupling capacitance is found from

$$C_c = \frac{1}{2} \left(C_o - C_e \right) \ \ [\text{F/m}] \tag{7}$$

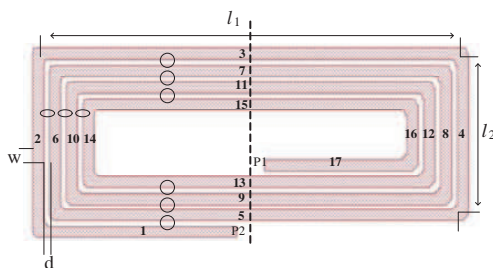After calculation of the coupling capacitances between the coupled

Figure 3. Segmentation of the spiral inductor for capacitance calculation.
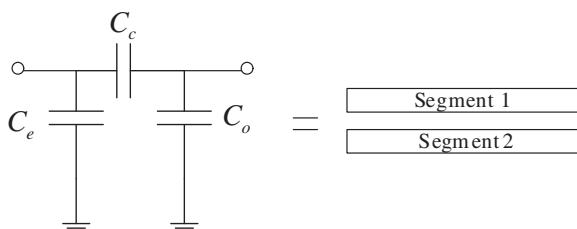

Figure 4. Equivalent circuit used for capacitance calculation between spiral segments.

spiral segments, the equivalent capacitance, C_{eq}, including the effect of all segments is found from network theory. The spiral inductor capacitance C_T is then found using the following relation.

$$C_T = 2C_{eq} + C_{o(\text{outside})} \ [\text{F/m}] \tag{8}$$

where $C_{o(\text{outside})}$ is the odd mode capacitance of the outside turn. All the capacitances are calculated per unit length. The series resistance $R(f)$ is found by assuming TEM wave propagation on the lines of the spiral inductor. The resistance, $R(f)$, then can be calculated as

$$R(f) = \frac{2}{w}\sqrt{\frac{\pi f \mu_c}{\sigma}} \ [\Omega/\text{m}] \tag{9}$$

μ_c and σ are the permeability and conductivity of the conductor which is used as a trace for the spiral inductor. R_p is the substrate resistance and calculated using

$$R_p = \frac{\rho l}{wh} \ [\Omega/\text{m}] \tag{10}$$

where w is the width of the trace, h is the thickness of the substrate and ρ is given in [25] for Al_2O_3. One port measurement network is obtained from the circuit shown in Fig. 2 by grounding the second port and illustrated in Fig. 5.

The quality factor, Q, and the resonant frequency, f_r, of the spiral inductor are important design parameters. They characterize the performance of the spiral inductor at the frequency of interest. These two parameters are calculated using the measurement circuit shown in Fig. 5. The expressions for the quality factor and the resonant frequency are given by Equations (11)–(12) as

$$Q = \frac{\text{Im}(Z)}{\text{Re}(Z)} \tag{11}$$

and

$$f_r = \frac{1}{2\pi\sqrt{L_T C_T}} \left[\frac{1 - R^2\left(\frac{C_T}{L_T}\right)}{1 - R_p^2\left(\frac{C_T}{L_T}\right)} \right]^{0.5} \tag{12}$$

2.2. Material Design

Spiral inductors designed and presented in this paper are used in the RF power amplifier system which operate at the HF range and deliver several kilowatts of power. The spiral inductors that are designed will be used as resonating inductor for the switched mode power amplifier, or filter inductor in the system. The material that is used as substrate for the spiral inductor should be able to handle the power dissipation during the operation. The power dissipation for each inductor that will be designed changes from 132 W to 675 W. The substrate material at the frequency of operation should present low loss and have high thermal conductivity. The best choice of the material exhibiting these features is Alumina (Al_2O_3). Thermal resistance of Al_2O_3 is found from
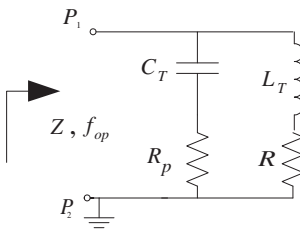
$$\theta_D = \frac{h}{kA} \, [°C/W] \tag{13}$$

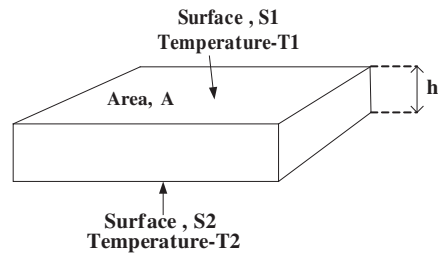**Figure 5.** Spiral inductor measurement circuit.

Figure 6. Material specimen for thermal calculation.

θ_D is the thermal resistance in $^\circ$C/W, h is thickness in inches, k is thermal conductivity of the substrate in Watts/(in$^\circ$C) and A is the area in in^2. Since $k = 0.6$[Watts/(in$^\circ$C)] is a known parameter, the thickness and the area of the substrate can be selected to meet with the required power dissipation. This can be better visualized on an arbitrary shaped material specimen shown in Fig. 6. Fig. 6 shows a layer of a thermally conductive material that has a constant cross sectional area A, thickness h, and thermal conductivity k. If the surface S_1 is maintained at a temperature T_1 and surface S_2 is maintained at a higher temperature T_2, then the dissipated power in the layer is defined as

$$P_D = \frac{T_2 - T_1}{\theta_T}[\text{W}] \tag{14}$$

The thermal resistance of a 0.1-in-thick Al$_2$O$_3$ for the required area is obtained as $\theta_D = 0.03^\circ$C/W. The purity of Al$_2$O$_3$ is given to be 96%. The metalization on the back and front of the substrate is composition of Copper, Nickel and Gold. The substrate material will be placed on a cold plate with an application of a thermal compound which has a thermal resistance around $\theta_C = 0.01^\circ$C/W. The substrate with thermal compound on the cold plate will present thermal resistance of $\theta_P = 0.07^\circ$C/W. This will increase overall thermal resistance of the configuration to $\theta_T = 0.11^\circ$C/W. Assuming the operating ambient temperature to be 50°C and the maximum power dissipation to be 675 W, the temperature of the substrate is calculated to be 124.25°C, which is 74.25°C above the ambient temperature. The flow rate of the coolant, coolant pressure, and coolant temperature for the cold plate are set to be 1.6 gpm, 60 psi, and 35°C to keep the ambient temperature at constant value. The power handling capacity of Al$_2$O$_3$ versus temperature including cold plate and thermal compound is illustrated in Fig. 7. Since the operating substrate temperature of Al$_2$O$_3$ can go up to 300°C, the calculated worst case temperature during operation is well below the safe operating range of the material. As a result, the substrate properties including physical dimensions such as thickness, surface area, and thermal characteristics can be determined for a reliable operation in our application using the method described above with the application of Equations (13) and (14).

3. NUMERICAL RESULTS

Based on the formulation introduced in Section 2.1, several spiral inductors are designed, simulated, and built using Al$_2$O$_3$ as a substrate with the method given in Section 2.2. Constructed microstrip spiral inductors are measured using HP 8753ES Network Analyzer. The
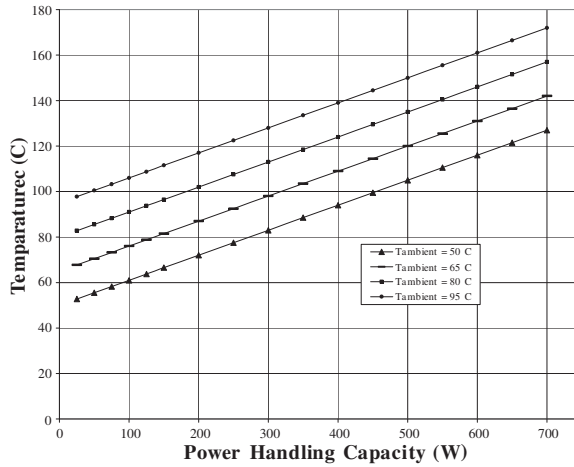
Figure 7. Power-handling capacity for of 0.1in thick Al_2O_3 including cold plate and thermal compound.

analytical results, simulation results, and experimental results are presented in the following subsections.

3.1. Analytical Results

Using the formulation given in Section 2.1, five spiral inductors are designed with different number of turns, trace width, spacing, conductor length and configurations. The substrate material is selected to be Alumina, Al_2O_3, with relative permittivity constant 9.8 and thickness 0.254 cm. The operational frequency for the inductors is 13.56 MHz, which is a common frequency for ISM applications. Table 1 illustrates the dimensions of the spiral inductors that are designed. An algorithm is developed using Mathcad to calculate the lumped element equivalent circuit element values and plot them on Smith Chart. Table 2 shows the analytical results for the calculated inductance value, and the resonant frequency for each inductor. The output of the developed program plotting the equivalent impedance on the Smith Chart for inductor 1 is shown in Fig. 8. During the operation of any RF system, spiral inductors are desired to have resonant frequencies approximately three times higher than the operational frequency of the system as a rule of thumb. The quality factor is needed to be high to avoid any thermal problems due to conductor and dielectric losses. Based on the analytical results, these two requirements are met for all of the inductors except the second inductor for the resonant frequency as shown in Table 2.
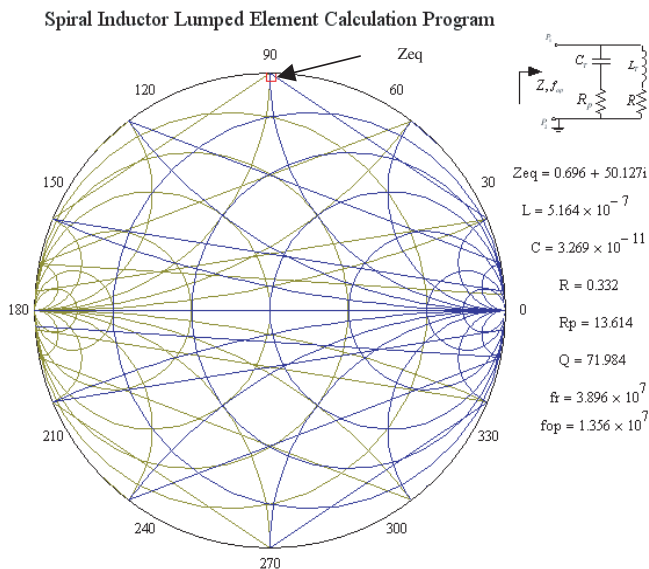
Figure 8. Spiral Inductor lumped element calculation program.

Table 1. Physical dimensions of spiral inductors.

	Trace With (cm)	Spacing (cm)	L_1 (cm)	L_2 (cm)
Ind 1	0.2032	0.1016	7.7	2.95
Ind 2	0.2032	0.0508	7.8	3
Ind 3	0.1524	0.0762	7.7	1.4
Ind 4	0.1524	0.0762	7.7	1.9
Ind 5	0.2032	0.3048	9.65	1.7

3.2. Simulation Results

Rectangular spiral inductors whose physical dimensions are given in Table 1 are simulated using MoM based planar electromagnetic simulator, Sonnet. Simulation results will be used to validate the analytical result and define the final configuration for the inductors that will be built. The layout of the simulated spiral inductors are illustrated in Fig. 9. Inductor 3 and inductor 4 are implemented on the same board. Inductor 5 is implemented as a symmetrical inductor also on a single board. Inductor 1 and inductor 2 are implemented on separate boards. Different configurations of the spirals inductors

Table 2. Analytical results for spiral inductors.

	Number of Turns	Inductance (nH)	Resonant Frequency Fr (MHz)
Ind 1	4	516.41	38.96
Ind 2	5	753.73	30.49
Ind 3	2.5	238.41	69.22
Ind 4	3.5	405.08	53.29
Ind 5	1.5	132.11	81.62

Table 3. Simulation Results for Spiral Inductors.

	Inductance (nH)	Resonant Frequency Fr (MHz)
Ind 1	529.76	40.8
Ind 2	741.41	33
Ind 3	244.6	77.2
Ind 4	392.97	54.25
Ind 5	132.78	92.5

that are illustrated in Fig. 9 demonstrate how to implement a spiral inductor based on the application to have optimum performance and results. Inductor 1 and Inductor 2 are used as components for filter in RF power amplifier (PA) system whereas Inductors 3, 4, and 5 are used as resonating inductors for RF PA. The simulation results for five spiral inductors are given in Table 3 .

Error between the simulation results and analytical results are given in Table 4. The maximum error in inductance calculation is found to be around 3%. The error increases to 11% for resonant frequency calculation. Please note that although our lumped element model and formulation for analytical calculation is one of the most involved model up to date using the most of the effects such as coupling capacitances, mutual inductances, substrate resistance, series resistance, skin effect, etc., it is still an approximate model with a certain level inaccuracy.

One of the biggest advantages of the simulation programs is the visualization of the current density distribution of the spiral inductor. The simulation result for the first inductor illustrating the current density distribution is given in Fig. 10. This is very important

Table 4. Error between simulation results and analytical results.

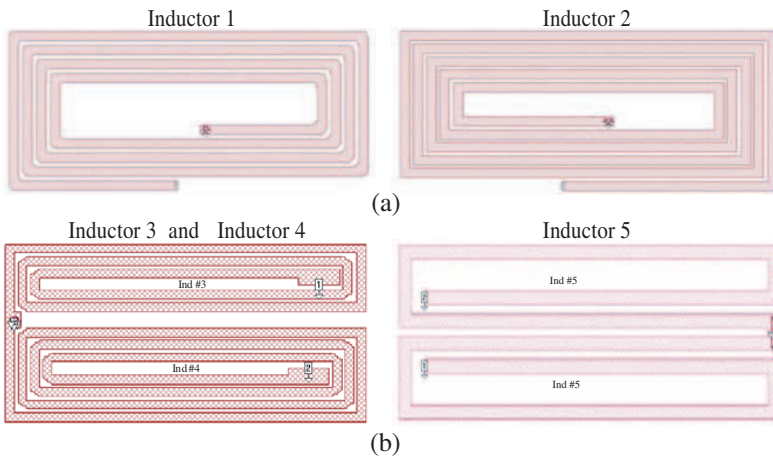|	Error in Inductance (%)	Error in Fr (%)
Ind 1	2.52	4.51
Ind 2	1.66	7.61
Ind 3	2.53	10.34
Ind 4	3.08	1.77
Ind 5	0.50	11.76

(a)

(b)

Figure 9. Layout of the spiral inductors that are simulated. (a) Inductor 1 and 2. (b) Inductor 3, 4 and 5.

information in practice, which can be used to adjust the spacing between the traces to prevent potential arcs during operation by distributing the voltage drop between the turns of the spiral at the desired level.

3.3. Experimental Results

The spiral inductors that are designed, and simulated are built and measured using network analyzer HP 8753ES. Fig. 11 illustrates the spiral inductors that are manufactured. The measurement results are given in Table 5 whereas the error between the measured, simulation and analytical results are given in Table 6. It has been observed that simulation results generally gave better error for inductance calculation, and resonant frequency for the spiral inductors.

However, it is worth to note that the error for the inductance value and resonant frequency were close between analytical, simulation
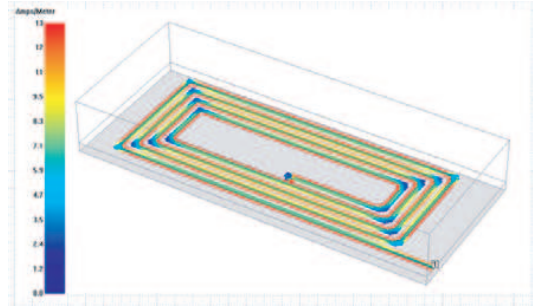

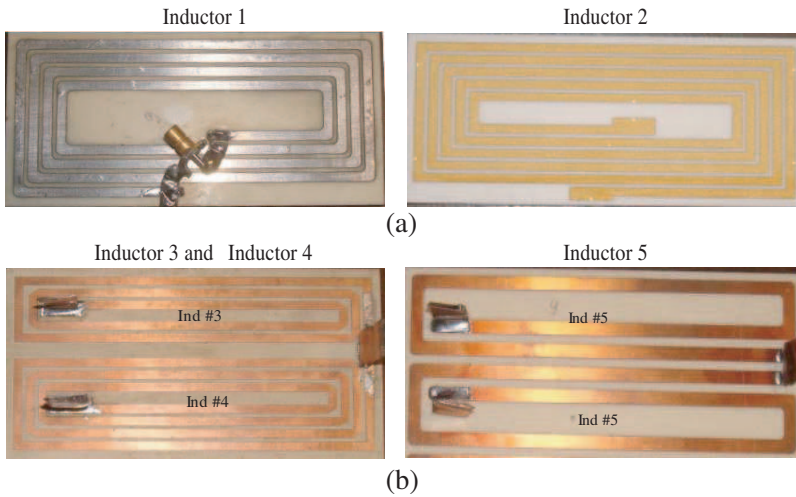**Figure 10.** Simulated spiral inductor showing current density.

Figure 11. The manufactured spiral inductors. (a) Inductor 1 and 2. (b) Inductor 3, 4 and 5.

Table 5. Measurement results.

	Inductance (nH)	Resonant Frequency Fr (MHz)
Ind 1	529.04	41.22
Ind 2	762.13	32.94
Ind 3	257.04	73.9
Ind 4	413.5	52.74
Ind 5	137.88	88.56

Table 6. Error between measured, simulation and analytical results.

	Measurement Inductance Value (nH)	Analytical Inductance Value (nH)	Simulation Inductance Value (nH)	Inductance Error (%) Measurement vs Analytical	Inductance Error (%) Measurement vs Simulation
Ind 1	529.04	516.41	529.76	2.45	0.14
Ind 2	762.13	753.73	741.41	1.11	2.79
Ind 3	257.04	238.41	244.6	7.81	5.09
Ind 4	413.5	405.08	392.97	2.08	5.22
Ind 5	137.88	132.11	132.78	4.37	3.84
	Measurement Resonant Frequency (MHz)	Analytical Resonant Frequency (MHz)	Simulation Resonant Frequency (MHz)	Fr Error (%) Measurement vs Analytical	Fr Error (%) Measurement vs Simulation
Ind 1	41.22	38.96	40.8	5.80	1.03
Ind 2	32.94	30.49	33	8.04	0.18
Ind 3	73.9	69.22	77.2	6.76	4.27
Ind 4	52.74	53.29	54.25	1.03	2.78
Ind 5	88.56	81.62	92.5	8.50	4.26

and experimental results. This confirms the accuracy of the proposed analytical method and developed algorithm to design spiral inductors at the HF range for ISM applications.

4. CONCLUSION

Analytical method and corresponding algorithm to design low profile microstrip spiral inductors for ISM applications at the HF range for high power applications are introduced. Based on the analytical results, five different spiral inductors are simulated using planar electromagnetic simulator, Sonnet, and built using 100 mil Alumina (Al_2O_3) substrate. Constructed spiral inductors are then measured with network analyzer HP 8735ES. The analytical, simulation and experimental results are then compared. The agreement has been observed on all the values. The implementation and thermal management methods for the spiral inductors for high power applications at the HF range are also given in detail. Practical and accurate analytical method that is introduced in this paper can be used to design spiral inductors for ISM applications at the HF range in the design of RF systems and components.

REFERENCES

1. Long, J. R. and M. A. Copeland, "The modeling, characterization, and design of monolithic inductors for silicon RF IC's," *IEEE J. of Solid-State Circuits*, Vol. 32, 357–369, 1997.

2. Niknejad, A. M. and R. G. Meyer, "Analysis, design, and optimization of spiral inductors and transformers for Si RF IC's," *IEEE J. of Solid-State Circuits*, Vol. 33, 1470–1481, 1998.

3. Reyes, A. C., S. M. El-Ghazaly, S. J. Dorn, M. Dydyk, D. K. Schroder, and H. Patterson, "Coplanar waveguides and

microwave inductors on silicon substrates," *IEEE Trans. on Microwave Theory and Tech.*, Vol. 43, 2016–2022, 1995.

4. Ashby, K. B., I. C. Koullias, W. C. Finley, J. J. Bastek, and S. Moinian, "High *Q* inductors for wireless applications in a complementary silicon bipolar process," *IEEE J. of Solid-State Circuits*, Vol. 31, 4–9, 1996.

5. Lu, L.-H., G. E. Ponchak, P. Bhattacharya, and L. P. B. Katehi, "High-Q X-band and K'-band micromachined spiral inductors for use in Si-based integrated circuits," *Proc. Silicon Monolithic Integrated Circuits RF Syst.*, 108–112, 2000.

6. Bahl, I. J., "Improved quality factor spiral inductor on GaAs substrates," *IEEE Microwave Guided Wave Lett.*, Vol. 9, 398–400, 1999.

7. Ribas, R. P., J. Lescot, J. L. Leclercq, N. Bernnouri, J. M. Karam, and B. Courtois, "Micromachined planar spiral inductor in standard GaAs HEMT MMIC technology," *IEEE Electron Device Lett.*, Vol. 19, 285–287, 1998.

8. Takenaka, H. and D. Ueda, "0.15 µm T-shaped gate fabrication for GaAs MODFET using phase shift lithography," *IEEE Trans. on Electron Devices*, Vol. 43, 238–244, 1996.

9. Chiou, M. H. and K. Y. J. Hsu, "A new wideband modeling technique for spiral inductors," *IET Microwave, Antennas, and Propagation*, Vol. 151, 115–120, 2006.

10. Lu, H.-C., T. B. Chan, C. C.-P. Chen, and C.-M. Liu, "LTCC spiral inductor synthesis and optimization with measurement verification," *IEEE Trans. on Advanced Packaging*, Vol. 33, 2010.

11. Talwalkar, N. A., C. P. Yue, and S. S. Wong, "Analysis and synthesis of on-chip spiral inductors," *IEEE Trans. on Electron Devices*, Vol. 52, 176–182, 2005.

12. Mukherjee, S., B. Mutnury, S. Dalmia, and M. Swaminathan, "Layout-level synthesis of RF inductors and filters in LCP substrate for Wi-Fi applications," *IEEE Trans. on Microwave Theory and Tech.*, Vol. 53, 2196–2210, 2005.

13. Kulkarni, J. P., C. Augustine, B. Jung, and K. Roy, "Nano spiral inductors for low-power digital spintronic circuits," *IEEE Trans. on Magnetics*, Vol. 46, 1898–1901, 2010.

14. Greenhouse, H. M., "Design of planar rectangular microelectronic inductors," *IEEE Transactions on Parts, Hybrids and Packaging*, Vol. 10, 101–109, 1974.

15. Jenei, S., B. K. J. C. Nauwelaers, and S. Decoutere, "Physics-based closed-form inductance expression for compact modeling

of integrated spiral inductors," *IEEE J. of Solid-State Circuits*, Vol. 37, 77–80, 2002.

16. Asgaran, S., "New accurate physics-based closed-form expressions for compact modeling and design of on-chip spiral inductors," *Proc. 14th Int. Conf. Microelectronics*, 247–250, 2002.

17. Mohan, S. S., M. M. Hershenson, S. P. Boyd, and T. H. Lee, "Simple accurate expressions for planar spiral inductance," *IEEE J. of Solid-State Circuits*, Vol. 34, 1419–1424, 1999.

18. Chen, C. C., J. K. Huang, and Y. T. Cheng, "A closed-form integral model of spiral inductor using the Kramers-Kronig relations," *IEEE Microwave AMD Wireless Comp. Letters*, Vol. 15, 2005.

19. Sieiro, J., J. M. Lopez-Villegas, J. Cabanillas, J. A. Osorio, and J. Samitier, "A physical frequency-dependent compact model for RF integrated inductors," *IEEE Trans. on Microwave Theory and Tech.*, Vol. 50, 384–392, 2002.

20. Sun, H., Z. Liu, J. Zhao, L. Wang, and J. Zhu, "The enhancement of Q-factor of planar spiral inductor with low-temperature annealing," *IEEE Trans. on Electron Devices*, Vol. 55, 931–936, 2008.

21. Tsai, H. S., J. Lin, R. C. Frye, K. L. Tai, M. Y. Lau, D. Kossives, F. Hrycenko, and Y. K. Chen, "Investigation of current crowding effect on spiral inductors," *IEEE MTT-S Symp. on Technologies to Wireless Applications*, 139–142, 1997.

22. Bushyager, N., M. Davis, E. Dalton, J. Laskar, and M. Tentzeris, "Q-factor and optimization of multilayer inductors for RF packaging microsystems using time domain techniques," *Electronic Components and Technology Conference*, 1718–1721, 2002.

23. Eroglu, A. and J. K. Lee, "The complete design of microstrip directional couplers using the synthesis technique," *IEEE Transactions on Instrumentation and Measurement*, Vol. 12, 2756–2761, 2008.

24. Costa, E. M. M., "Parasitic capacitances on planar coil," *Journal of Electromagnetic Waves and Applications*, Vol. 23, Nos. 17–18, 2339–2350, 2009.

25. Aluminum Oxide Material Properties: http://accuratus.com/alumox.html.